EasyChair Preprint

№ 9221

The Influence of Human Walking Activities on the Doppler Characteristics of Non-Stationary Indoor Channel Models

Muhammad Muaaz, Ahmed Abdel-Gawwad and Matthias Pätzold

November 2, 2022

The Influence of Human Walking Activities on the Doppler Characteristics of Non-Stationary Indoor Channel Models

Muhammad Muaaz, Ahmed Abdelgawwad, and Matthias Pätzold

Faculty of Engineering and Science, University of Agder
P.O. Box 509, 4898 Grimstad, Norway
{muhammad.muaaz,ahmed.abdel-gawwad,matthias.paetzold}@uia.no

Abstract. This paper analyzes the time-variant (TV) Doppler power spectral density of a 3D non-stationary fixed-to-fixed indoor channel simulator after feeding it with realistic trajectories of a walking person. The trajectories of the walking person are obtained by simulating a full body musculoskeletal model in OpenSim. We provide expressions of the TV Doppler frequencies caused by these trajectories. Then, we present the complex channel gain consisting of fixed scatterers and a cluster of moving scatterers. After that, we use the concept of the spectrogram to analyze the TV Doppler power spectral density of the complex channel gain. Finally, we present expressions of the TV mean Doppler shift and Doppler spread. The work of this paper is important for human activity recognition systems using radio-frequency (non-wearable) sensors as the demand for such systems has increased nowadays.

Keywords: non-stationary channel model, OpenSim, musculoskeletal model, dynamic simulation, spectrogram, time-frequency distributions

1 Introduction

Human activity recognition (HAR) aims at inferring human activities from body motion and gesture data recorded by different types of wearable and non-wearable sensors. Systems with the ability to automatically recognize human activities can significantly improve and simplify our daily living in an increasingly complex society. Motivated by this, HAR is not only a well-researched, but still a very active research area mainly due to its dynamic nature, wide variety of applications, advancements in learning algorithms, and developments in sensing technologies. Depending on the type of sensors, HAR systems can be divided into vision-based [4, 9], sensor-based [7, 18], and device-free systems [14, 15].

Vision-based systems record and process videos and still images of users to recognize their activities. They require a line-of-sight (LOS) link and may lead to possible violations of the user's privacy.

Sensor-based systems use inexpensive sensors, such as inertial measurement units (IMUs) to capture human movement data. However, users need to carry these sensors all the time for continuous activity recognition. Furthermore, the performance of sensor-based systems is susceptible to the placement of the sensors on the human body. In

the device-free approaches, such as radio-frequency (RF) sensing, the transmitter and receivers are placed in the environment and they continuously transmit and receive RF signals. These RF signals are very sensitive to the change in the domestic environment. Human movements in the environment introduce fluctuations in the RF signals. These variation-enriched RF signals are picked up by the receivers and used for activity recognition [15]. Since device-free HAR systems suffer less from privacy issues and do not require the users to carry sensors all the time, the device-free approach has become a preferred choice for applications such as health and indoor HAR systems for the elderly.

In recent years, various device-free HAR systems have been developed [14–17]. Although the existing device-free HAR systems have shown promising results, they face a major challenge, namely *limited capability to deal with changes in the environment* [6]. This is because RF signals picked up by the receivers usually carry information about the moving and non-moving scatterers[1] present in the environment. As a result, a HAR system trained by using the data collected from specific subjects in a specific environment may not perform well when applied to a different environment to recognize activities of other individuals. To overcome this challenge, researchers have proposed several ideas. For instance, Jiang et al. [17] used environment and subject-independent features to train HAR models. This approach requires training data to be collected from various subjects under different environmental settings. In [16], a semi-supervised learning approach is used to address this issue, where users are required to manually label the new instances of recorded channel state information (CSI) data upon detecting changes in the CSI-fingerprints of the activities. This approach requires manual interaction from users which is not feasible in various environment, such as public places and hospitals.

Radio communication researchers have proposed a three-dimensional (3D) indoor channel modeling[2] technique, which captures the Doppler effect caused by the body movements, for device-free HAR [1, 2]. The basic idea is that fixed scatterers and different movements of moving scatterers affect the Doppler characteristics of the channel differently. After filtering out the effect of fixed scatterers on the Doppler characteristics of the channel, we can obtain Doppler signatures for different activities, which can be used for environment-independent activity recognition. The additional advantage of this approach is that the measurements from the simulated channel can be used to train the learning algorithms without additional efforts for the collection of training data.

The contribution of this paper is the analysis of the Doppler power spectrum characteristics of a 3D non-stationary fixed-to-fixed (F2F) indoor channel simulator, which is fed with the trajectories of major body parts. For this purpose, we first simulate the human walking activity by using a full-body musculoskeletal model to obtain trajectories of different body parts, e.g., torso, pelvis, upper arms, lower arms, hands, upper legs, lower legs, and toes. Then, we model these moving body parts of the walking human by a cluster of synchronized moving scatterers. After that, we compute the time-variant (TV) Doppler frequencies caused by the trajectories of these major body parts. Further-

[1] Here scatterers mean objects present in the environment. When a radio wave hits an object with a rough surface, then the wave will be redirected in many directions depending on the slope of the object.

[2] A channel model is a physical layer model of the mathematical representation of the effects of a communication channel through which RF signals propagate.

more, the expression of the instantaneous channel phase of each moving scatterer of the cluster is provided. Next, we present an expression of the complex channel gain of the 3D non-stationary F2F multipath fading channel with fixed scatterers and a cluster of synchronized moving scatterers. In addition, expressions of the TV mean Doppler shift and TV Doppler spread are presented. In this paper, we use the spectrogram approach to analyze the influence of a cluster of moving scatterers on the TV Doppler power spectrum. The spectrogram consists of two terms: the auto-term and the cross-term. The auto-term represents the desired Doppler power spectrum, while the cross-term represents an undesired interference term, which reduces the resolution of the spectrogram. Finally, we provide expressions for the TV mean Doppler shift and TV Doppler spread computed by using the spectrogram.

The rest of this paper is organized as follows. Section 2, succinctly explains the dynamic simulation of human walking activities. Section 3 presents the TV Doppler frequencies caused by the walking person, the complex channel gain, TV mean Doppler shift, TV Doppler spread, and the spectrogram of the complex channel gain. Section 4 discusses the numerical results of the spectrogram of the complex channel gain fed by the trajectories of the body parts of a walking human. Section 5 summarizes our work and proposes possible extensions for future work.

2 Simulation of Human Walking Activities

To study the influence of human walking activities on the Doppler characteristics of the indoor channel model, we need to obtain trajectories of human body parts during walking activities. Instead of defining and validating our own trajectory models for different human body parts, in this paper, we have used an OpenSim-based full-body musculoskeletal model to obtain realistic trajectories of human body parts.

2.1 Overview of OpenSim and its general workflow

OpenSim [5] is a publicly available open-source suit of tools for modeling musculoskeletal structures and analyzing dynamic simulation of a wide range of human movements [3] in rehabilitation science [8], sports science [10], and robotics research [11]. OpenSim provides a large repository of musculoskeletal models consisting of rigid bodies, joints, and specialized forces. The skeleton is modeled by rigid bodies which are interconnected by joints. Joints define the motion of a rigid body with respect to its parent rigid body and specialized force elements are used to model the muscles of human bodies.

The first step in simulating any human movement in OpenSim is to formally define the dynamic musculoskeletal model and its interactions with the environment. Once the model is formulated, it is scaled by using the scaling tool of OpenSim. In the scaling process, the dimensions and mass properties of each body segment as well as the musculotendon properties (e.g., muscle fiber length) of the dynamic musculoskeletal model are scaled to match with the anthropometric data of real subjects [3, 5].

In the next step, the inverse kinematics (IK) tool is used to find the generalized coordinates (including joint angels and positions) of the dynamic musculoskeletal model.

At each time step, the IK tool computes the generalized coordinates that describes the model in a pose which "best matches" the experimental/motion-capture data at each time step [3, 5]. At this stage, the measured ground reaction forces (GRFs) and joint moments are usually inconsistent with the model kinematics. To overcome this issue a residual reduction algorithm (RRA) is applied. The goal of the RRA is to make measured GRFs and moments more consistent with the model kinematics [3,5]. Thereafter, the computed muscle control (CMC) tool is used to compute muscle excitations that drive the generalized coordinated muscle-driven simulation of the movement [3,5].

2.2 Trajectories of body parts of a moving person

In this paper, we have employed a validated full-body musculoskeletal model and the experimental motion data from a previously published work by Rajagopal et al. [13]. This model consists of a bony geometry of the full body, 37 degrees of freedom (DoF), hill-type muscle models to model 80 musculotendon units actuating the lower body, and 17 ideal torque actuators for the upper body [13], as shown in Fig. 1.

The authors in this study [13] collected motion data using 41 retroreflective markers measured at a sampling rate of 100 Hz by using an eight-camera optical motion-capture system. GRFs and moments were measured with ground force plates at a sampling rate of 2000 Hz, and the EMG data were recorded by placing wireless surface electrodes on 10 different muscles. Further details about the dynamic model and data collection process can be found in [13]. First, the full-body musculoskeletal model is scaled according to the experimental data, then the general workflow of OpenSim (see Section 2.1) is followed to generate the dynamic simulation of the full gait cycle. Finally, the body kinematics analysis is performed to obtain the TV kinematics (including position and velocity) of the center of mass (CoM) of each body segment defined in the full body

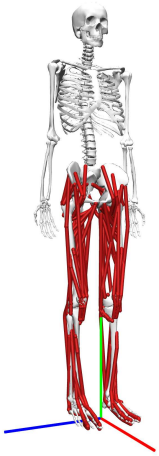

Fig. 1. A full body musculoskeletal model [x-axis (red), y-axis (green), and z-axis (blue)].

musculoskeletal model as shown in Fig. 2. The TV velocity vectors $\boldsymbol{v}_n(t)$ of CoM of each body segment are fed to the channel simulator described in Section 3 to compute the complex channel gain of the RF channel in presence of a walking human.

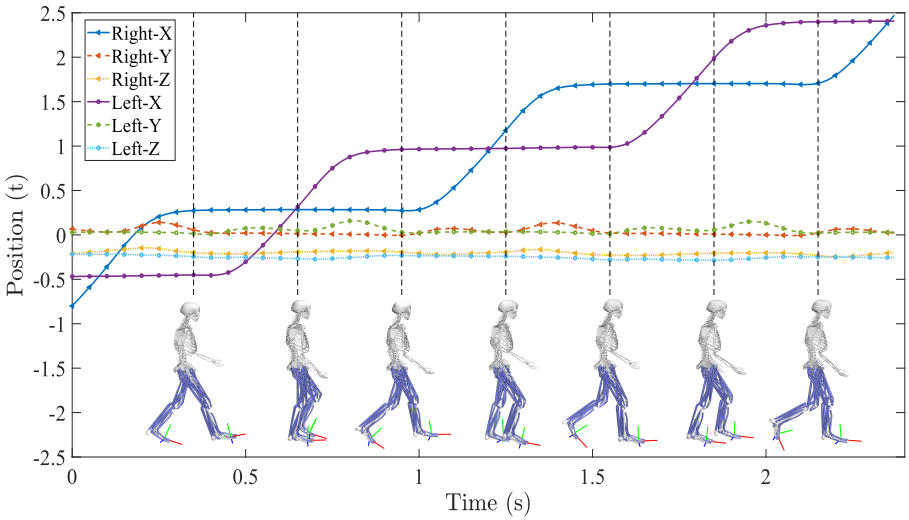

Fig. 2. 3D displacement of the CoM of the right and left toes during walking.

3 Monitoring Human Activity Using the Spectrogram

The trajectories of the major body parts discussed in Section 2 vary in time and space. In this section, we explore the impact of these temporal and spatial variations on the Doppler characteristics of the received signal. This is done by simulating the complex channel gain of F2F indoor channels with these trajectories generated in Section 2.2 as inputs. Then, the Doppler spectral characteristics of the complex channel gain are analyzed by using the concept of the spectrogram.

3.1 The complex channel gain

Figure 3 shows a multipath propagation scenario of an F2F 3D indoor channel. In this scenario, we have a fixed transmitter (T_x) and a fixed receiver (R_x) located at $\left(x^T,\, y^T,\, z^T\right)$ and $\left(x^R,\, y^R,\, z^R\right)$, respectively. We assume that the LOS is obstructed and both T_x and R_x are equipped with omnidirectional antennas. The considered scenario includes fixed objects, such as walls and furniture. These fixed objects are simply modelled by M-fixed point scatterers S_m^{F} for $m = 1, 2, \ldots, \mathcal{M}$. Fig. 3 also shows a moving person modelled by a cluster of N-synchronized moving scatterers S_n^{M}, where $n = 1, 2, \ldots, \mathcal{N}$. Each moving scatterer S_n^{M} represents a moving body part, which has

a trajectory described by its TV velocity vector $\boldsymbol{v}_n(t)$ (see Section 2.2). Single bounce scattering is assumed, i.e., each wave arriving at R_x is scattered by either a fixed scatterer S_m^{F} or a moving scatterer S_n^{M}.

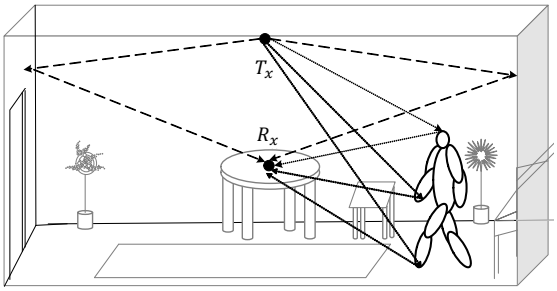

Fig. 3. A 3D non-stationary indoor multipath propagation scenario with fixed transmitter T_x, fixed receiver R_x, a moving person, and fixed objects, such as walls and furniture.

The Doppler frequency influenced by the nth moving scatterer S_n^{M} of the cluster is given by [1]

$$\begin{aligned} f_n(t) = -\frac{\mathrm{V}_n\left(t\right) f_0}{c_0} \times \Bigg\{ & \cos\left(\beta_{v_n}\left(t\right)\right) \left[\cos\left(\beta_n^T(t)\right) \cos\left(\alpha_n^T(t) - \alpha_{v_n}\left(t\right)\right) \right. \\ & \left. + \cos\left(\beta_n^R(t)\right) \cos\left(\alpha_{v_n}\left(t\right) - \alpha_n^R(t)\right) \right] \\ & + \sin\left(\beta_{v_n}\left(t\right)\right) \times \left[\sin\left(\beta_n^T(t)\right) + \sin\left(\beta_n^R(t)\right) \right] \Bigg\} \end{aligned} \tag{1}$$

where the functions $\beta_{v_n}(t)$, $\alpha_{v_n}(t)$, $\beta_n^T(t)$, $\alpha_n^T(t)$, $\beta_n^R(t)$, and $\alpha_n^R(t)$ denote the TV horizontal angle of motion (HAOM), vertical angle of motion (VAOM), elevation angle of departure (EAOD), vertical angle of departure (AAOD), elevation angle of arrival (EAOA), and azimuth vertical angle of (AAOA) of the nth moving scatterer S_n^{M}, respectively. The expressions of these functions are obtained by using the inverse trigonometric functions. Further details about these expressions are provided in [1]. The function $\mathrm{V}_n(t) = |\boldsymbol{v}_n(t)|$ designates the TV speed of the motion of the nth moving scatterer of the cluster. The parameters f_0 and c_0 are the carrier frequency of the signal and the speed of light, respectively. The instantaneous channel phase influenced by the nth moving scatterer of the cluster is expressed as [12]

$$\theta_{n,\mathrm{M}}(t) = 2\pi \int_{-\infty}^{t} f_n(t')dt' = 2\pi \int_{0}^{t} f_n(t')dt' + \theta_{n,\mathrm{M}} \tag{2}$$

where the first term of the right-hand side of (2) is the TV phase shift influenced by the motion of the nth moving scatterer of the cluster of the moving person. The second term $\theta_{n,\mathrm{M}}$ designates the initial phase shift which is modelled as a zero-mean random variable with uniform distribution with values from $-\pi$ to π, i.e., $\theta_{n,\mathrm{M}} \sim \mathcal{U}\left(-\pi,\, \pi\right]$. Thus, the

instantaneous channel phase $\theta_{n,\mathrm{M}}(t)$ in (2) is a stochastic process. The complex channel gain $\mu(t)$ that consists of $\mathcal{N}+\mathcal{M}$ received multipath components can be expressed as [1]

$$\mu(t) = \sum_{n=1}^{\mathcal{N}} c_{n,\mathrm{M}}\, e^{j\theta_{n,\mathrm{M}}(t)} + \sum_{m=1}^{\mathcal{M}} c_{m,\mathrm{F}}\, e^{j\theta_{m,\mathrm{F}}}. \tag{3}$$

The first term in (3) represents the superposition of the received $\mathcal{N}$ waves corresponding to the moving scatterers. Each path in the first term of (3) is described by a constant path gain $c_{n,\mathrm{M}}$ and a stochastic phase process $\theta_{n,\mathrm{M}}(t)$ due to the motion of the moving scatterer. The second term represents the superposition of $\mathcal{M}$ received multipath components originating from the fixed scatterers. Each component in the second term is associated with a constant path gain $c_{m,\mathrm{F}}$ and a random phase $\theta_{m,\mathrm{F}}$ caused by the interaction with the fixed scatterer. The random variables $\theta_{n,\mathrm{M}}$ and $\theta_{m,\mathrm{F}}$ are independent and identically distributed (i.i.d.) with uniform distribution from $-\pi$ and π, i.e., $\theta_{m,\mathrm{F}},\, \theta_{n,\mathrm{M}} \sim \mathcal{U}\,(-\pi,\, \pi]$. The expression of the complex channel gain $\mu(t)$ given by (3) is a stochastic model for a 3D non-stationary F2F multipath fading channel with fixed scatterers and a cluster of moving scatterers. The TV mean Doppler shift and TV Doppler spread by the model described by (3) are given by [12]

$$B_f^{(1)}(t) = \frac{\sum\limits_{n=1}^{\mathcal{N}} c_{n,\mathrm{M}}^2\, f_n(t)}{\sum\limits_{n=1}^{\mathcal{N}} c_{n,\mathrm{M}}^2 + \sum\limits_{m=1}^{\mathcal{M}} c_{m,\mathrm{F}}^2} \tag{4}$$

and

$$B_f^{(2)}(t) = \sqrt{\frac{\sum\limits_{n=1}^{\mathcal{N}} c_{n,\mathrm{M}}^2\, f_n^2(t)}{\sum\limits_{n=1}^{\mathcal{N}} c_{n,\mathrm{M}}^2 + \sum\limits_{m=1}^{\mathcal{N}} c_{m,\mathrm{F}}^2} - \left(B_f^{(1)}(t)\right)^2} \tag{5}$$

respectively.

3.2 Spectrogram of the complex channel gain

To compute the TV Doppler power spectrum by using the spectrogram approach, a sliding window is required. In this paper, a Gaussian window described by

$$h(t) = \frac{1}{\sqrt{\sigma_w \sqrt{\pi}}} e^{-\frac{t^2}{2\sigma_w^2}} \tag{6}$$

is used, where the parameter σ_w is called the window spread. The window function $h(t)$ is positive, even, and has normalized energy, i.e., $\int_{-\infty}^{\infty} h^2(t) = 1$. Then, we compute the Fourier transform of the multiplication of the complex channel gain and the sliding window to obtain the short-time Fourier transform (STFT) $X(f,t)$. Finally, the STFT

$X(f,t)$ is multiplied by its complex conjugate, which defines the spectrogram $S_\mu(f,t)$ as

$$S_\mu(f,t) \;=\; |X(f,t)|^2 \;=\; S_\mu^{(a)}(f,t) + S_\mu^{(c)}(f,t). \tag{7}$$

The spectrogram $S_\mu(f,t)$ in (7) consists of two terms, the auto-term $S_\mu^{(a)}(f,t)$ and the cross-term $S_\mu^{(c)}(f,t)$. The auto-term $S_\mu^{(a)}(f,t)$ represents the desired TV Doppler power spectral density. It is a real and positive function. The cross-term $S_\mu^{(c)}(f,t)$ represents an undesired spectral interference component, which is also real, but not necessarily positive. It reduces the resolution of the spectrogram. Further details about the expressions of $X(f,t)$, $S_\mu^{(a)}(f,t)$, and $S_\mu^{(c)}(f,t)$ can be found in [1]. It should be noted that the cross-term can be eliminated by taking the average of the spectrogram $S_\mu(f,t)$ over the random phase variables $\theta_{n,\mathrm{M}}$ and $\theta_{m,\mathrm{F}}$, i.e., $E\left\{S_\mu(f,t)\right\}|_{\theta_{n,\mathrm{M}},\theta_{m,\mathrm{F}}} = S_\mu^{(a)}(f,t)$. The TV mean Doppler shift and Doppler spread can be computed from the spectrogram using the following expressions [2]

$$B_\mu^{(1)}(t) = \frac{\int\limits_{-\infty}^{\infty} f S_\mu(f,t) df}{\int\limits_{-\infty}^{\infty} S_\mu(f,t) df} \tag{8}$$

and

$$B_\mu^{(2)}(t) = \sqrt{\frac{\int\limits_{-\infty}^{\infty} f^2 S_\mu(f,t) df}{\int\limits_{-\infty}^{\infty} S_\mu(f,t) df} - \left(B_\mu^{(1)}(t)\right)^2} \tag{9}$$

respectively.

4 Numerical Results

In this section, we will discuss the numerical results of the spectrogram $S_\mu(f,t)$, the auto-term $S_\mu^{(a)}(f,t)$ of the spectrogram, the TV mean Doppler shift, and TV Doppler spread. For the simulation scenario in Fig. 4, we have chosen a room with the dimensions $10\,\mathrm{m} \times 5\,\mathrm{m} \times 2.4\,\mathrm{m}$. For the locations of T_x and R_x, we chose the coordinates $(5\,\mathrm{m},\ 2.5\,\mathrm{m},\ 2.3\,\mathrm{m})$ and $(5\,\mathrm{m},\ 3\,\mathrm{m},\ 2.3\,\mathrm{m})$, respectively. The number of the fixed scatterers $\mathcal{M}$ was chosen to be 6. With respect to Fig. 4, a person is walking parallel to the x-axis, towards the positive direction as a cluster of 18 moving scatterers, i.e., $\mathcal{N} = 18$. The path gains of each moving and fixed scatterer have been computed by

$$c_{n,\mathrm{M}} = \sqrt{\frac{2\eta}{\mathcal{N}}} \qquad \text{and} \qquad c_{m,\mathrm{F}} = \sqrt{\frac{2\,(1-\eta)}{\mathcal{M}}} \tag{10}$$

where the parameter η is used to balance the contribution of the moving scatterers in the cluster and the fixed scatterers to the fading power. Its value was set to 0.6. The

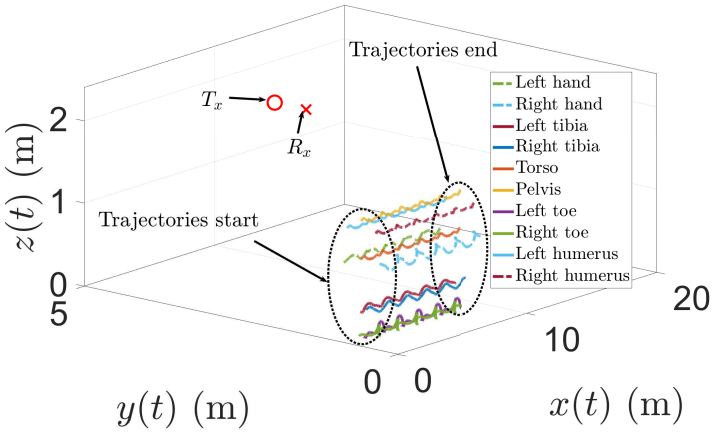

Fig. 4. 3D indoor simulation scenario showing the trajectories of the body parts (moving scatterers) of a walking person.

value for the carrier frequency f_0 was chosen to be 5.9 GHz. The indoor F2F channel simulator was monitoring the walking person for 6 ss. The TV VAOMs $\beta_{v_n}(t)$ and TV HAOMs $\alpha_{v_n}(t)$ were computed from the TV velocities of the moving scatterers. The TV EAODs $\beta_n^T(t)$ and AAODs $\alpha_n^T(t)$ of the moving scatterers were calculated from their TV displacements and the location of T_x. Also, the TV EAOAs $\beta_n^R(t)$ and AAOAs $\alpha_n^R(t)$ of the moving scatterers were computed from their TV displacements and the location of R_x. Then, the Doppler frequencies of the moving scatterers were computed using (1). For computing the spectrogram, the window spread parameter σ_w of the Gaussian window function $h(t)$ was set to 0.01 s. The values of the random channel phases $\theta_{n,\mathrm{M}}$ and $\theta_{m,\mathrm{F}}$ were obtained as outcomes from random generators with uniform distributions from $-\pi$ and π.

Figure 5 depicts the spectrogram $S_\mu(f,t)$ given by (7), showing the variations of the TV Doppler power spectrum. However, they are blurred due to the effect of the cross-term $S_\mu^{(c)}(f,t)$, which reduces the resolution of the spectrogram $S_\mu(f,t)$. Figure 6 shows the auto-term $S_\mu^{(a)}(f,t)$ of the spectrogram. The influence of the moving cluster on the TV Doppler power spectrum is clearly visible. The Doppler frequencies approach zero values at $t \approx 3.2$ s. The reason is that, at this time instant, the values of the TV EAODs $\beta_n^T(t)$, AAODs $\alpha_n^T(t)$, TV EAOAs $\beta_n^R(t)$, AAOAs $\alpha_n^R(t)$ of the moving scatterers tend to $-\pi/2$ rad.

Figure 7 depicts the TV mean Doppler shifts $B_f^{(1)}(t)$ and $B_\mu^{(1)}(t)$ calculated as expressed in (4) and (8), respectively. The expression of the TV mean Doppler shift $B_\mu^{(1)}(t)$ given by (8) was applied to the spectrogram $S_\mu(f,t)$ and the auto-term $S_\mu^{(a)}(f,t)$. The variations of $B_\mu^{(1)}(t)$ calculated by using $S_\mu(f,t)$, are due to the impact of the cross-term $S_\mu^{(c)}(f,t)$. There is a good match between $B_\mu^{(1)}(t)$ and $B_f^{(1)}(t)$. The depicted functions in Fig. 7 approach zero-mean values at $t \approx 3.2$ s as the values of the TV EAODs $\beta_n^T(t)$, AAODs $\alpha_n^T(t)$, TV EAOAs $\beta_n^R(t)$, and AAOAs $\alpha_n^R(t)$ of the moving scatterers tend to $-\pi/2$ rad.

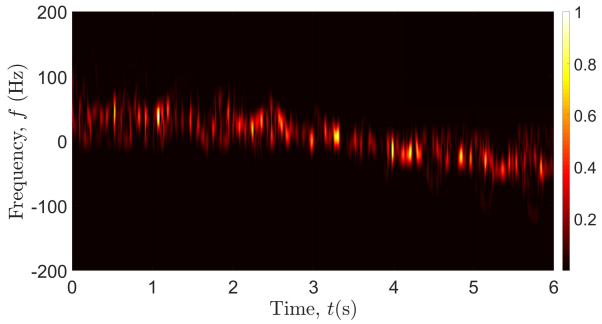

Fig. 5. Spectrogram $S_\mu(f,t)$ of the complex channel gain $\mu(t)$ given by (7).

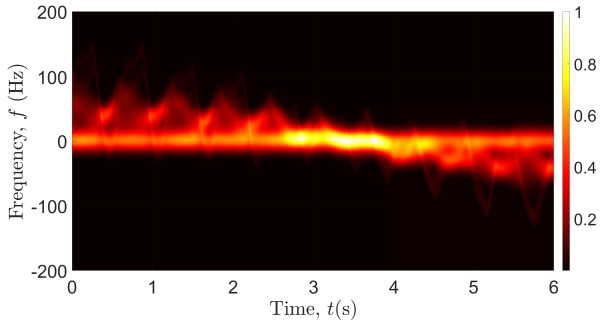

Fig. 6. The auto-term $S_\mu^{(a)}(f,t)$ of the spectrogram of the complex channel gain $\mu(t)$.

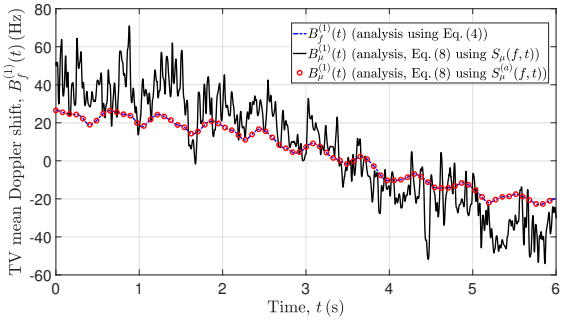

Fig. 7. TV mean Doppler shifts $B_f^{(1)}(t)$ and $B_\mu^{(1)}(t)$ given by (4) and (8), respectively.

Figure 8 depicts the TV Doppler spreads $B_f^{(2)}(t)$ and $B_\mu^{(2)}(t)$ calculated by using (5) and (9), respectively. The expression of TV Doppler spread $B_\mu^{(2)}(t)$ given by (8) was applied to the spectrogram $S_\mu(f,t)$ and the auto-term $S_\mu^{(a)}(f,t)$. The fluctuations of $B_\mu^{(2)}(t)$ calculated by using $S_\mu(f,t)$ are due to the impact of the cross-term $S_\mu^{(c)}(f,t)$. The functions $B_\mu^{(2)}(t)$ computed by utilizing the auto-term $S_\mu^{(a)}(f,t)$ and $B_f^{(2)}(t)$ do not match closely due to the influence of the Gaussian window spread σ_w on $B_\mu^{(2)}(t)$.

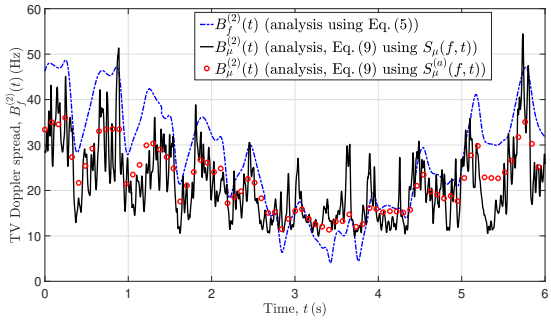

Fig. 8. TV Doppler spreads $B_f^{(2)}(t)$ and $B_\mu^{(2)}(t)$ computed by using (5) and (9), respectively.

5 Conclusion

In this paper, we studied the influence of human walking activity on the Doppler characteristics of an F2F non-stationary indoor channel model. At first, we used a full-body musculoskeletal model to simulate human walking activity to obtain trajectories of different body parts. We modelled the walking human as a cluster of synchronized moving scatterers. After that, we used the trajectories as inputs for this channel simulator to compute the Doppler frequencies caused by the walking human. The influence of the walking person on the TV Doppler power spectral density was shown by means of the spectrogram of the complex channel gain. Moreover, we analyzed the impact of the walking human on the TV mean Doppler shift and TV Doppler spread derived from the spectrogram. The results demonstrated the influence of the walking person on the Doppler power spectral characteristics. In the future, we will study the influence of activities such as sitting and running as well as the detection of events such as falling on the Doppler characteristics of the channel.

Acknowledgement

This work is carried out within the scope of WiCare project funded by the Research Council of Norway under the grant number 261895/F20.

References

1. Abdelgawwad, A., Pätzold, M.: A framework for activity monitoring and fall detection based on the characteristics of indoor channels. In: IEEE 87th Vehicular Technology Conference (VTC Spring). Porto, Portugal (Jun 2018)
2. Abdelgawwad, A., Pätzold, M.: On the influence of walking people on the Doppler spectral characteristics of indoor channels. In: 2017 IEEE 28th Annual International Symposium on Personal, Indoor, and Mobile Radio Communications (PIMRC). pp. 1–7. IEEE (2017)
3. Delp, S.L., Anderson, F.C., Arnold, A.S., Loan, P., Habib, A., John, C.T., Guendelman, E., Thelen, D.G.: OpenSim: Open-source software to create and analyze dynamic simulations of movement. IEEE Transactions on Biomedical Engineering 54(11), 1940–1950 (Nov 2007)

4. Harville, M., Li, D.: Fast, integrated person tracking and activity recognition with plan-view templates from a single stereo camera. In: Proceedings of the 2004 IEEE Computer Society Conference on Computer Vision and Pattern Recognition. pp. 398–405. CVPR'04, IEEE Computer Society, Washington, DC, USA (2004)
5. Hicks, J.: OpenSim documentation (2018), https://simtk-confluence.stanford.edu/x/pga9AQ, (last accessed) 19.02.2019.
6. Jiang, W., Miao, C., Ma, F., Yao, S., Wang, Y., Yuan, Y., Xue, H., Song, C., Ma, X., Koutsonikolas, D., Xu, W., Su, L.: Towards environment independent device free human activity recognition. In: Proceedings of the 24th Annual International Conference on Mobile Computing and Networking. pp. 289–304. MobiCom '18, ACM, New York, NY, USA (2018)
7. Kwapisz, J.R., Weiss, G.M., Moore, S.A.: Activity recognition using cell phone accelerometers. SIGKDD Explor. Newsl. 12(2), 74–82 (Mar 2011)
8. Lessard, S., Pansodtee, P., Robbins, A., Trombadore, J.M., Kurniawan, S., Teodorescu, M.: A soft exosuit for flexible upper-extremity rehabilitation. IEEE Transactions on Neural Systems and Rehabilitation Engineering 26(8), 1604–1617 (Aug 2018)
9. Li, H., Cohen, I.: Inference of human postures by classification of 3D human body shape. In: 2003 IEEE International Workshop on Analysis and Modeling of Faces and Gestures (AMFG). vol. 00, p. 74 (10 2003)
10. Mahadas, S., Mahadas, K., Hung, G.K.: Biomechanics of the golf swing using OpenSim. Computers in Biology and Medicine 105, 39 – 45 (2019)
11. Maldonado, G., Souères, P., Watier, B.: From biomechanics to robotics. In: Biomechanics of Anthropomorphic Systems, pp. 35–63. Springer (2019)
12. Pätzold, M., Gutiérrez, C.A., Youssef, N.: On the consistency of non-stationary multipath fading channels with respect to the average Doppler shift and the Doppler spread. In: Proc. IEEE Wireless Communications and Networking Conference, WCNC 2017. San Francisco, CA, USA (Mar 2017)
13. Rajagopal, A., Dembia, C.L., DeMers, M.S., Delp, D.D., Hicks, J.L., Delp, S.L.: Full-body musculoskeletal model for muscle-driven simulation of human gait. IEEE Transactions on Biomedical Engineering 63(10), 2068–2079 (Oct 2016)
14. Sigg, S., Scholz, M., Shi, S., Ji, Y., Beigl, M.: RF-sensing of activities from non-cooperative subjects in device-free recognition systems using ambient and local signals. IEEE Transactions on Mobile Computing 13(4), 907–920 (April 2014)
15. Wang, W., Liu, A.X., Shahzad, M., Ling, K., Lu, S.: Device-free human activity recognition using commercial WiFi devices. IEEE Journal on Selected Areas in Communications 35(5), 1118–1131 (May 2017)
16. Wang, Y., Liu, J., Chen, Y., Gruteser, M., Yang, J., Liu, H.: E-eyes: Device-free location-oriented activity identification using fine-grained WiFi signatures. In: Proceedings of the 20th Annual International Conference on Mobile Computing and Networking. pp. 617–628. MobiCom '14, ACM, New York, NY, USA (2014)
17. Wei, B., Hu, W., Yang, M., Chou, C.T.: From real to complex: Enhancing radio-based activity recognition using complex-valued CSI. CoRR abs/1804.09588 (2018)
18. Yatani, K., Truong, K.N.: Bodyscope: A wearable acoustic sensor for activity recognition. In: Proceedings of the 2012 ACM Conference on Ubiquitous Computing. pp. 341–350. UbiComp '12, ACM, New York, NY, USA (2012)